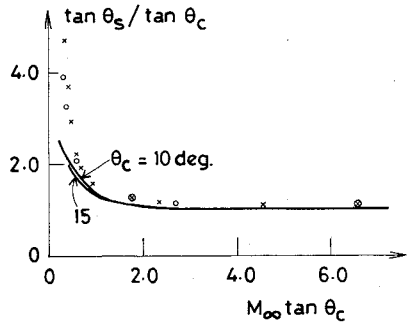


**Fig. 2 Comparison for shock-wave angle $\theta_s$ for a cone: ○, × exact (○, 10 deg; ×, 15 deg); ——, Eq. (11a); $\gamma = 1.405$.**

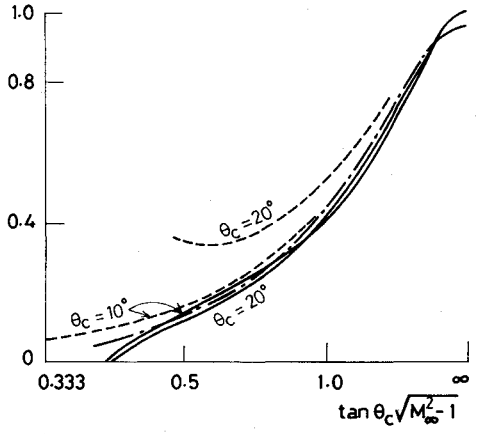


**Fig. 3 Comparison for ratio of shock wave to body initial curvature $\nu$ for a parabolic ogive: - - -, exact; ——, HSDT; ——, Eq. (8d); $\gamma = 1.405$.**

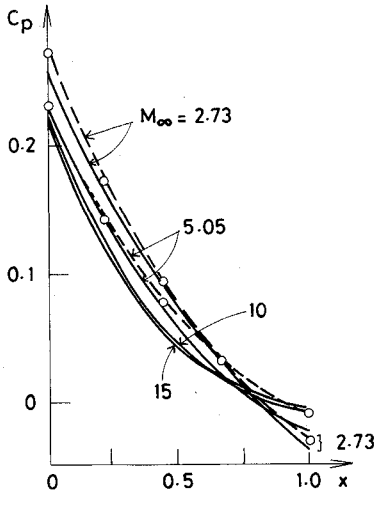


**Fig. 4 Comparison for $C_p$ on a parabolic ogive of fineness ratio 3: ○, experiment; - - -, method of characteristics; ——, Eq. (19); $\gamma = 1.405$.**

good if $M_\infty \tan\theta_c$ is $O(1)$ or greater. In Fig. 3, the ratio of shock wave to body initial curvature, $\nu$, is compared with exact calculations and with the HSDT for a class of ogives ($m = 1$ and $k = B/2$). The figure shows good agreement with the exact calculations for $\theta_c = 10$ deg.

Figure 4 compares Eq. (19) with experiment and the method of characteristics. Notice the good agreement even for $M_\infty = 2.73$. The figure also shows that increasing $M_\infty$ has a moderate decreasing effect for the front part of the body and a moderate increasing effect on the very rear part.

## Conclusions

Very good results are obtained for pointed-nose slender axisymmetric bodies at zero incidence. The agreement with the exact method and experiment covers a wide range of $\gamma$, $M_\infty$, and $k$. The analysis relies on a recent formulation of the hypersonic small disturbance theory, where the equations have been reduced here to ordinary differential equations. The main advancement of the present hypersonic theory lies in having a smaller number of unknown functions and easier equations that lend themselves to further analytical study.

## References

[1]Sedov, L. I., *Similarity and Dimensional Methods in Mechanics,* Academic, New York, 1959, Chap. 4, (English translation).

[2]Mirels, H., *Hypersonic Flow over Slender Bodies Associated with Power-Law Shocks,* Vol. 7, Advances in Applied Mechanics, 1962.

[3]Cole, J. D., and Aroesty, J., "Hypersoic Similarity Solutions for Airfoils Supporting Exponential Shock Waves," *AIAA Journal,* Vol. 8, 1970, pp. 308-315.

[4]Hui, W. H., "A Solution for Hypersonic Flow Past Slender Bodies," *Journal of Fluid Mechanics,* Vol. 48, Pt. 1, 1971, pp. 23-31.

[5]Hui, W. H., and Hemdan, H. T., "Higher Order Similarity Solutions for Hypersonic Flow Past Airfoils," *Proceedings of the International Conference on Symmetry, Similarity and Group Theoretic Methods in Mechanics,* Univ. of Calgary, Canada, May 1974, pp. 403-417.

[6]Hemdan, H. T., "Newtonian Flow over Axisymmetric Bodies," *Transactions of the Japan Society of Aeronautical and Space Sciences,* Vol. 32, No. 95, 1989, pp. 13-25.

[7]Jischke, M. C., and Kim, B. S., "Hypersonic Flow Past an Axisymmetric Body with Small Longitudinal Curvature," *AIAA Journal,* Vol. 20, No. 10, 1982, pp. 1346-1351.

[8]Sims, J. L., "Tables for Supersonic Flow Around Right Circular Cones at Zero Angles of Attack," NASA SP-3004, 1964.

# Resonance Prediction for Slotted Circular Wind Tunnel Using Finite Element

In Lee* and Ki-Young Baik†
*Korea Advanced Institute of Science and Technology, Daejon, Korea*

## Introduction

MODEL flutter and unsteady airload measurements will be affected by resonant phenomena. When the model frequency is near a wind-tunnel resonant frequency, the results of these test will be inaccurate. Widmayer et al.[1] conducted some experiments to measure the oscillatory aerodynamic forces and moments acting on a rectangular wing. The test results were in considerable error near the tunnel resonant frequency. Clevenson and Widmayer[2] also observed the occurrence of resonance in experiments on a two-dimensional wing. Therefore, it is important to predict the wind-tunnel resonant frequency accurately.

Davis and Moore[3] and Acum[4] have obtained the resonance frequencies for the rectangular cross section. Lee[5] has obtained the resonance frequencies for a rectangular and an octagonal cross section by using finite elements.

Some wind tunnels have circular cross sections. Also, many wind tunnels have several slots on the wall to reduce model

Received March 9, 1990; revision received Aug. 6, 1990; accepted for publication Aug. 21, 1990. 

*Associate Professor, Department of Aerospace Engineering, 373-1, Kusung-dong, Yusung-ku. Member AIAA.

†Mechanical Engineer, Kia Motors Corporation.

blockage effects. This Note gives the resonance analysis for a circular cross section with slots. It is very difficult to predict the resonant frequencies for a slotted wind tunnel analytically. In this case, the finite element method is very useful.

## Finite Element Formulation

For a test section of a wind tunnel shown in Fig. 1, the following governing equation can be obtained from Ref. 5:

$$p_{xx} + p_{yy} + \left(\frac{\omega}{a_e}\right)^2 p = 0 \tag{1}$$

where $p$ is a perturbation pressure, $\omega$ is the angular frequency, and $a_e$ is the effective speed of sound [defined as $a_o(1 - M^2)^{1/2}$ where $a_o$ is the speed of sound of a fluid medium]. The boundary condition on the solid wall is given as

$$\frac{\partial p}{\partial n} = 0 \tag{2}$$

The pressure outside the tunnel wall is assumed equal to the freestream pressure. The perturbation pressure outside the tunnel wall is assumed to be very small, and the boundary condition at the outside of a slot is assumed to be equivalent to $p = 0$. Many investigators use the foregoing boundary condition ($p = 0$) at a slot in accordance with the usual practice in tunnel-interference theory.[6,7]

The appropriate functional for a wind tunnel can be written as[5]

$$F = \frac{1}{2\rho a_e^2}\int_v p^2\,dv - \frac{1}{2\rho\omega^2}\int_v (\nabla p)^2\,dv \tag{3}$$

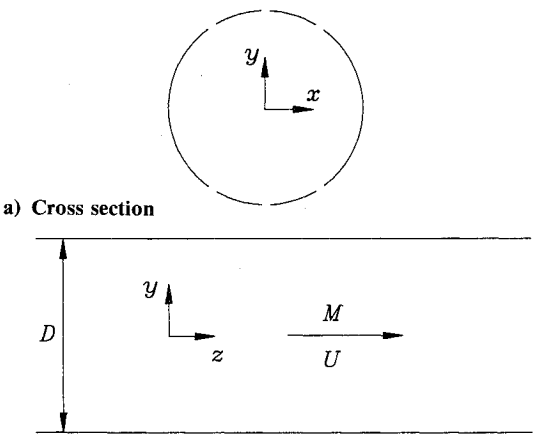


**Fig. 1 Circular wind tunnel.**

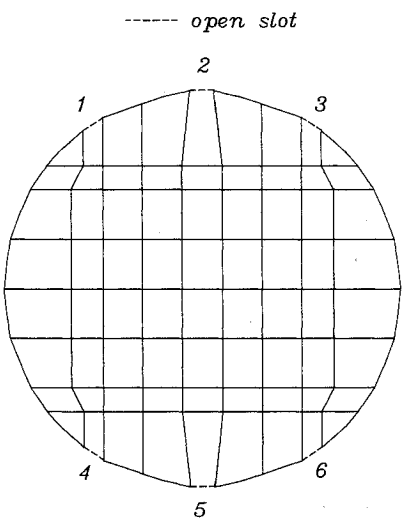


**Fig. 2 Finite element mesh for circular wind tunnel with slots.**

Setting the first variation of this functional, $F$, to zero leads to the governing equation (1) and the boundary condition (2). The pressure within each element $v_i$ can be approximated by shape functions

$$p = [N]_i\{p\}_i \tag{4}$$

Substituting Eq. (4) into Eq. (3), we can get the functional $F_i$ for element $v_i$.

$$F_i = \frac{1}{2\rho\omega^2}\left(\omega^2\{p\}_i^T[k]_i\{p\}_i - \{p\}_i^T[m]_i\{p\}_i\right) \tag{5}$$

where $[m]_i$ is the mass matrix and $[k]_i$ is the stiffness matrix

$$[m]_i = \int_{v_i}[B]_i^T[B]_i\,dv \tag{6}$$

$$[k]_i = \frac{1}{a_e^2}\int_{v_i}[N]_i^T[N]_i\,dv \tag{7}$$

$$[B]_i = \begin{Bmatrix} \dfrac{\partial}{\partial x} \\ \dfrac{\partial}{\partial y} \\ \dfrac{\partial}{\partial z} \end{Bmatrix}[N]_i \tag{8}$$

The first variation of Eq. (5) gives the following eigenvalue problem for subvolume $v_i$:

$$[m]_i\{p\}_i - \omega^2[k]_i\{p\}_i = \{0\} \tag{9}$$

If we assemble the subelements, we get the eigenvalue problem for the complete volume $V$

$$[M]\{P\} - \omega^2[K]\{P\} = \{0\} \tag{10}$$

where $[M]$ is the mass matrix for the complete system and $[K]$ is the stiffness matrix for the complete system. For this analysis, two-dimensional isoparametric eight-node elements are used to calculate element mass and stiffness matrices.

## Results and Discussion

Figure 2 shows finite element mesh for the circular cross-sectional wind tunnel. Its radius is 1 m. Dashed lines represent slots. The convergence test of two-dimensional eight-node elements has been performed for the circular cross section given in Fig. 2 when all the slots are closed. The computational results were compared with the analytical solution given in Ref. 8. Twelve elements were sufficient for convergence. Figure 3 shows the resonant frequencies when one slot each on top and bottom (central slots, slots 2 and 5 of Fig. 2) is open. The open area ratio of the slots, $e$, is defined as $2d/\pi R$, where $R$ is the radius of the cross section and $d$ is the slot width. The nondimensional resonant frequency is defined as $\omega R/\beta a_o$, where $\omega$ is the resonant frequency, $a_o$ is the speed of sound of the fluid medium, and $\beta$ is $(1 - M^2)^{1/2}$. Circular symbols correspond to the horizontal vibration mode and triangular symbols correspond to the vertical vibration mode. When a wind-tunnel model such as an airplane main wing is installed horizontally in the test section, unsteady motion of the model couples with the vertical vibration mode. As the oscillating model frequency approaches the resonant frequency, the vertical vibration motion of the model will be strongly affected by the vertical vibration (resonance) mode. Therefore, the vertical vibration mode is very important. As the open ratio increases, the vertical vibration frequency also increases, but the horizontal vibration frequency increases only slightly. Hence, in the case of one slot (central slot), the influence of the slot size on the horizontal vibration is very small but the influence on the vertical vibration is relatively large. When the other

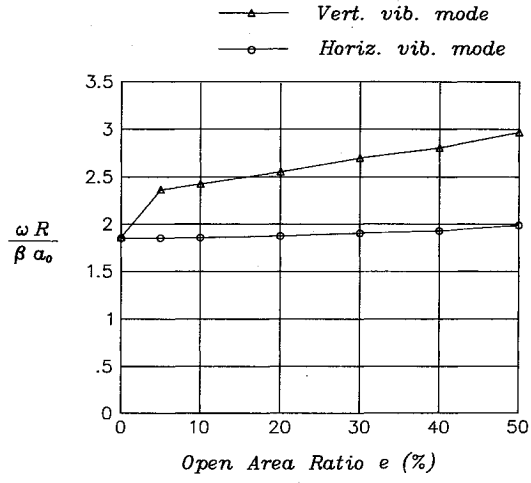


**Fig. 3 Resonant frequencies for circular wind tunnel with one slot each on top and bottom.**

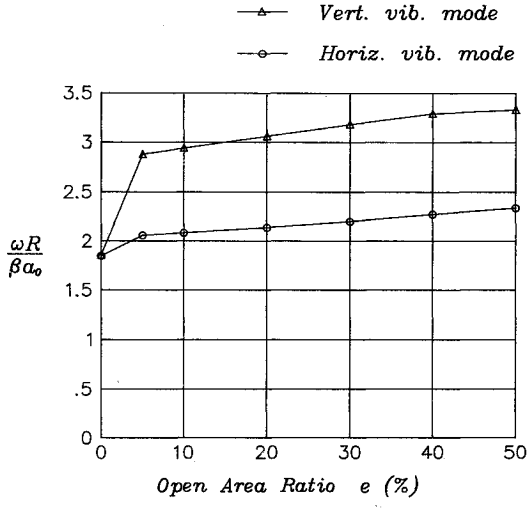


**Fig. 4 Resonant frequencies for circular wind tunnel with three slots each on top and bottom.**

pair of slots (slots 1 and 4, for example) are open, the vertical vibration frequency will decrease and the horizontal vibration frequency will increase. The central slots will affect the vertical vibration mode more effectively than the other pairs of slots. The other pairs of slots will affect the horizontal vibration mode more than the central slots.

Figure 4 shows the resonant frequencies when three slots each on top and bottom (slot numbers 1–6 of Fig. 2) are open. In this figure, the open area ratio of the slots, $e$, is defined as $6d/\pi R$. Both horizontal and vertical frequencies increase as the slot open ratio increases. The influence of three slots on the horizontal vibration is larger than that of one slot. For the same open ratio, the vertical and the horizontal vibration frequencies for three slots are higher than those for one slot.

Figure 5 illustrates the resonant frequencies for both one and three slots when the open ratio is 10%. As Mach number increases, vertical and horizontal vibration frequencies decrease. For the vertical vibration mode, the resonant frequency for three slots is the highest and that for closed slots is the lowest. Three distributed slots each on the top and the bottom side affect the vertical vibration mode more effectively than one central slot each on the top and the bottom for the same open area ratio. Therefore, both the number and the position of slots affect the vertical vibration frequencies significantly. For the horizontal vibration mode, the frequency for three slots is highest, but the frequency for one slot is almost the same as that for a closed slot. Hence, the central

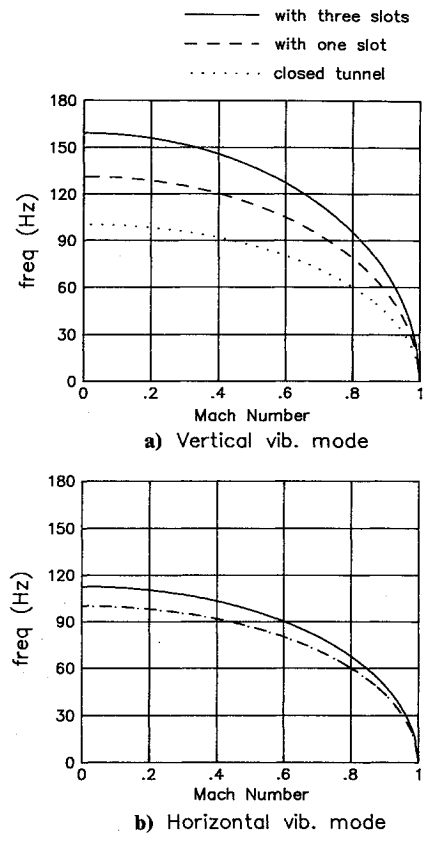


**Fig. 5 Effect of slots and Mach number on resonant frequencies for circular wind tunnel.**

slot (one slot open) does influence the vertical vibration mode, but does not influence the horizontal vibration mode. Three slots influence both the horizontal and the vertical vibration. These phenomena are different from those for the rectangular wind tunnel.[5]

## Conclusions

An eight-node finite element analysis gives accurate results. For the same open ratio, the resonant frequencies (both horizontal and vertical vibration mode) for three slots are higher than those for one slot. Three slots influence both the horizontal and the vertical vibration mode, but one slot (central slot) influences the vertical vibration mode only. The slots on the vertical centerline affect the vertical vibration mode effectively. The slots away from the vertical centerline are less effective in the vertical vibration mode, but more effective in the horizontal vibration mode than the central slots.

## References

[1]Widmayer, E., Clevenson, S. A., and Leadbetter, S. A., "Some Measurements of Aerodynamic Forces and Moments at Subsonic Speeds on a Rectangular Wing of Aspect Ratio 2 Oscillating about the Midchord," NACA TN-4240, 1958.

[2]Clevenson, S. A., and Widmayer, E., "Experimental Measurements of Forces and Moments of a Two-Dimensional Oscillating Wing at Subsonic Speeds," NACA TN-3686, 1956.

[3]Davis, D. D., and Moore, D., "Analytical Study of Blockage and Substitution of an Equivalent Homogeneous Boundary for the Discrete Slots," NASA R.M.-L53E07b, 1953.

[4]Acum, W. E. A., "A Simplified Approach to the Phenomenon of Wind Tunnel Resonance," Aeronautical Research Council, Rept. and Memo 3371, 1962.

[5]Lee, I., "Resonance Prediction for Closed and Open Wind Tunnel by the Finite Element Method," *AIAA Journal,* Vol. 27, No. 4, 1989, pp. 391–398.

[6]Acum, W. E. A., "Subsonic Wind Tunnel Wall Corrections," AGARDograph 109, 1966, Chap. 4.

[7]Garner, H. C., Moore, A. W., and Wight, K. C., "The Theory of Interference Effects on Dynamic Measurements in Slotted-Wall Tunnels at Subsonic Speeds and Comparisons with Experiment," Aeronautical Research Council, Rept. and Memo 3500, 1966.

[8]Kinsler, L. E., Frey, A. R., Coppens, A. B., and Sanders, J. V., *Fundamentals of Acoustics*, Wiley, New York, 1982.

# Enhancement of Frequency and Damping in Large Space Structures with Extendible Members

C. T. Sun* and R. T. Wang†
*Purdue University, West Lafayette, Indiana 47907*

## Introduction

WHEN disturbed, a large space structure (LSS) is likely to continue vibrating for some time because of its low frequencies and possibly small damping. Therefore, the objective of vibration control is to design the structure and its control to reduce dynamic responses in this structure. An effective way to achieve this goal is using damping augmentation that can be obtained by active or passive means. Juang[1] added a vibration absorber at the tip of a truss beam to produce the effect of passive damping augmentation. Balas[2] used an Euler-Bernoulli beam to illustrate active damping augmentation by direct velocity feedback of collocated/noncollocated sensors and actuators. Aubrun[3] used both direct feedback of velocity and displacement to change the modal frequencies and damping ratio of a structure. Meirovitch[4] extended the concept to modal space control of a distributed system.

Usually, in active damping-augmentation design, the sensors, actuators, and filters are mounted externally on the structure. The design requires a knowledge of elastic modal frequencies and modal shapes at the locations of sensors and actuators. However, these frequencies and shapes are very difficult to obtain in zero-gravity environment. Also, the vibrational modes of such structures are numerous, densely packed, and of low frequencies compared to the onboard controller bandwidth.

In contrast to the conventional control of a structure, the use of extendible truss members allows one to vary the control force internally. In this paper, the equations of motion for a truss with extendible members are derived. The effectiveness of using extendible truss members to tailor the vibrational characteristics of an LSS is investigated. Furthermore, a truss beam subjected to transient loading is used as an example to illustrate the effect of extendible truss members.

## Formulation

Consider an extendible truss element consisting of an extending-contracting device which is assumed to be short in length compared with the length of the truss bar (see Fig. 1). The total elongation of the bar is given by

$$\Delta = \Delta_1 + \Delta_0 \tag{1}$$

where $\Delta_1$ is the elongation of the elastic bar and $\Delta_0$ is produced by the extending-contracting device. The corresponding total strain is

$$\epsilon = \epsilon_1 + \epsilon_0 \tag{2}$$

where $\epsilon_1 = \Delta_1/L$ and $\epsilon_0 = \Delta_0/L$. If damping is added to the element, then the stress in the truss bar is given by

$$\sigma(t) = E\epsilon(t) + c\dot{\epsilon}(t) - \sigma_0(t) \tag{3}$$

where $\sigma_0(t) = E\epsilon_0(t) + c\dot{\epsilon}_0(t)$ is the perturbing stress produced by the extension-contraction actuator, $E$ is Young's modulus, $\dot{\epsilon}(t)$ is the strain rate, and $c$ is a viscous damping coefficient.

The finite element formulation is achieved based on the following displacement function with respect to the local coordinates:

$$u(x, t) = u_1(t)(1 - x/L) + u_2(t)x/L$$

$$v(x, t) = v_1(t)(1 - x/L) + v_2(t)x/L \tag{4}$$

where $u_i$ and $v_i$ are the horizontal and vertical displacements, respectively, at the $i$th node.

Following the standard procedure, the equations of motion for the truss element are derived as

$$\begin{bmatrix} f_1 \\ q_1 \\ f_2 \\ q_2 \end{bmatrix} + \begin{bmatrix} -1 \\ 0 \\ 1 \\ 0 \end{bmatrix} A\sigma_0 = \frac{EA}{L}\begin{bmatrix} 1 & 0 & -1 & 0 \\ 0 & 0 & 0 & 0 \\ -1 & 0 & 1 & 0 \\ 0 & 0 & 0 & 0 \end{bmatrix}\begin{bmatrix} u_1 \\ v_1 \\ u_2 \\ v_2 \end{bmatrix}$$

$$+\frac{cA}{L}\begin{bmatrix} 1 & 0 & -1 & 0 \\ 0 & 0 & 0 & 0 \\ -1 & 0 & 1 & 0 \\ 0 & 0 & 0 & 0 \end{bmatrix}\begin{bmatrix} \dot{u}_1 \\ \dot{v}_1 \\ \dot{u}_2 \\ \dot{v}_2 \end{bmatrix}$$

$$+\frac{\rho AL}{6}\begin{bmatrix} 2 & 0 & 1 & 0 \\ 0 & 2 & 0 & 1 \\ 1 & 0 & 2 & 0 \\ 0 & 1 & 0 & 2 \end{bmatrix}\begin{bmatrix} \ddot{u}_1 \\ \ddot{v}_1 \\ \ddot{u}_2 \\ \ddot{v}_2 \end{bmatrix} \tag{5}$$

where $f_i$ and $q_i$ are the vertical and horizontal nodal forces, respectively, at the $i$th joint. The axial force in the truss member is given by

$$S = \frac{EA}{L}[-1 \quad 0 \quad 1 \quad 0]\begin{bmatrix} u_1 \\ v_1 \\ u_2 \\ v_2 \end{bmatrix}$$

$$+\frac{cA}{L}[-1 \quad 0 \quad 1 \quad 0]\begin{bmatrix} \dot{u}_1 \\ \dot{v}_1 \\ \dot{u}_2 \\ \dot{v}_2 \end{bmatrix} - q_0 \tag{6}$$

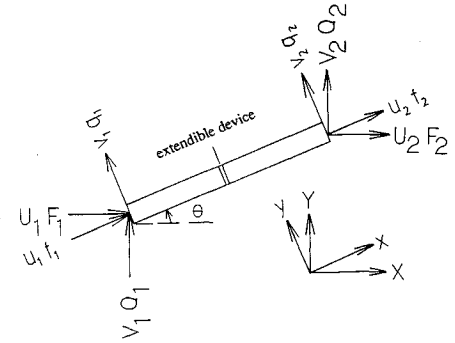


**Fig. 1 A truss member with extension-contraction device.**

Presented as Paper 88-2482 at the AIAA SDM Issues of the International Space Station Conference, Williamsburg, VA, April 21–22, 1988; received May 10, 1988; revision received Oct. 10, 1990; accepted for publication Nov. 29, 1990. 

*Professor, School of Aeronautics and Astronautics. Associate Fellow AIAA.

†Graduate Student; currently Associate Professor, Department of Engineering Sciences, National Cheng Kung University, Taiwan, Republic of China.